

Layer and spontaneous polarizations in perovskite oxides and their interplay in multiferroic bismuth ferrite

Nicola A. Spaldin,¹ Ipek Efe,¹ Marta D. Rossell,² and Chiara Gattinoni¹

¹*Department of Materials, ETH Zurich, CH-8093 Zürich, Switzerland*

²*Electron Microscopy Center, Swiss Federal Laboratories for Materials Science and Technology, Empa, 8600, Dübendorf, Switzerland*

(Dated: February 26, 2021)

We review the concept of surface charge, first in the context of the polarization in ferroelectric materials, and second in the context of layers of charged ions in ionic insulators. While the former is traditionally discussed in the ferroelectrics community, and the latter in the surface science community, we remind the reader that the two descriptions are conveniently unified within the modern theory of polarization. In both cases, the surface charge leads to electrostatic instability — the so-called “polar catastrophe” — if it is not compensated, and we review the range of phenomena that arise as a result of different compensation mechanisms. We illustrate these concepts using the example of the prototypical multiferroic bismuth ferrite, BiFeO_3 , which is unusual in that its spontaneous ferroelectric polarization and its layer charges can be of the same magnitude. As a result, for certain combinations of polarization orientation and surface termination its surface charge is self-compensating. We use density functional calculations of BiFeO_3 slabs and superlattices, analysis of high-resolution transmission electron micrographs as well as examples from the literature to explore the consequences of this peculiarity.

I. INTRODUCTION

Bound charge at the surface of an insulator, or at an interface between two insulating materials, must be screened in order to avoid a so-called polar catastrophe caused by a divergence of the electrostatic energy [1]. Such bound surface charge, σ_{surf} , exists whenever there is an uncompensated component of the bulk polarization, \vec{P}_{bulk} , perpendicular to a surface, and is given by

$$\sigma_{\text{surf}} = \vec{P}_{\text{bulk}} \cdot \vec{n} \quad (1)$$

where \vec{n} is the unit vector along the surface normal. A bulk polarization can occur of course in ferroelectric materials due to their *spontaneous polarization*. It can also occur in centrosymmetric crystals in which the ions form charged layers; we refer to this latter contribution as the *layer polarization*.

Many mechanisms are known for screening bound surface charge, ranging from metal electrodes [2, 3], to formation of charged defects [4–8] or adsorption of charged species [9–12], and even loss or reorientation of ferroelectric polarization [13–15]. Note that it is not possible to screen the bound surface charge by surface relaxation alone, without the addition or removal of charged species.

In this work we explore the special case of multiferroic perovskite-structure bismuth ferrite, BiFeO_3 , which has both a spontaneous polarization from its ferroelectric distortion and a layer polarization from its ionic charges. BiFeO_3 is particularly unusual because the size of its spontaneous ferroelectric polarization in the common [001] and [111] growth directions is close to the size of the layer polarization from the charged ionic layers in flat (100) and (111) planes. As a result, for certain choices of polarization orientation and surface ter-

mination, the spontaneous and layer polarizations self-compensate, leading to uncharged surfaces that are stable without external screening mechanisms.

We begin by reviewing in the next section (Sec. II) two key results of the modern theory of polarization — the multivaluedness of the polarization lattice and the concept of the polarization quantum — that are key to this work. We then briefly review compensating mechanisms at the surfaces of ferroelectric materials with charge-neutral layers (Sec. III). Next, we discuss centrosymmetric materials with charged layers (Sec. IV), and show how the layer polarization associated with charged ionic layers is conveniently described within the modern theory of polarization. We then combine the concepts of layer polarization and spontaneous polarization in the example of bismuth ferrite (Sec. V), discussing in turn its interface with metallic electrodes, and with insulators with different layer polarizations.

II. REMINDER OF KEY RESULTS FROM THE MODERN THEORY OF POLARIZATION

We begin with a reminder of a fundamental result of the modern theory of polarization [16], that the polarization, \vec{P} , of a bulk periodic solid, is not a single number but rather a *lattice* of values, separated by the polarization quantum, $\vec{P}_q = \frac{e\vec{R}}{V}$. The polarization quantum corresponds to the change in polarization on moving an electronic charge e by a lattice vector \vec{R} (V is the unit cell volume), which changes the polarization by an amount \vec{P}_q , but does not change the physical system. (For a more extensive introductory discussion, see Ref. 17.)

A consequence of this property is that the polarization

lattice of a centrosymmetric crystal, which must also be centrosymmetric by symmetry, can take one of two sets of values,

$$\vec{P} = 0 + n\vec{P}_q \quad , \quad \text{or} \quad (2)$$

$$\vec{P} = \frac{\vec{P}_q}{2} + n\vec{P}_q \quad , \quad (3)$$

where n is any integer. All insulating, centrosymmetric, periodic solids can be classified as belonging to one of these classes, which we will refer to as having “zero-containing” (Eq. 2) or “half-quantum-containing” (Eq. 3) polarization lattices. (In principle, it is possible for a centrosymmetric material to contain zero for one component of its polarization and a half quantum along another component, although we do not know of an example). Examples of half-quantum-containing centrosymmetric crystals are the high-symmetry paraelectric phase of BiFeO₃, and the wide-band-gap insulating perovskite, LaAlO₃. Note also that these materials have charged ionic layers perpendicular to their usual [001] growth direction; in section IV we will show that these properties are formally connected. SrTiO₃ is an example of the zero-containing polarization lattice type; correspondingly charge-neutral layers, such as SrO and TiO₂ (001) planes, can be readily identified.

While the fact that a centrosymmetric crystal can have a polarization lattice that does not contain zero is somewhat unintuitive, it is reconciled by a second important result of the modern theory of polarization: *Differences* in polarization, defined as the change in polarization along a given branch of the polarization lattice as the system is modified along an insulating pathway, are single-valued. As a result, the spontaneous polarization, which is the difference in polarization between the ferroelectric structure and its high-symmetry centrosymmetric counterpart, is single-valued. Since only polarization differences (for example when a ferroelectric is switched between domains, or heated above its Curie temperature) are experimentally accessible, the theory is consistent with experimental reality. Indeed, when discussing the properties of infinite, bulk periodic crystals, the question of whether the polarization lattice contains zero or a half quantum is not generally relevant.

At surfaces and interfaces, however, the question of the origin of the polarization lattice should not be disregarded. The bulk polarization, \vec{P}_{bulk} , which gives rise to the bound charge at the surface of a crystal (Eqn. 1) contains the contributions from both the half-polarization quantum (layer charges) *and* the spontaneous polarization [18]. Considering only the spontaneous polarization in evaluating the bound charge on the surface of a material will yield an incorrect result for centrosymmetric crystals with half-quantum-containing polarization lattices, as well as for ferroelectrics whose paraelectric reference structures’ polarization lattices contain the half quantum.

To illustrate these concepts in this work, we use ABO₃ perovskite-structure oxides in the usual pseudo-cubic

[001] growth orientation. (For the generalization to other surface planes see Ref. 1). In this orientation, the layers have alternating AO / BO₂ chemistry, and the planar surfaces are formed from either entirely AO or entirely BO₂ layers. Since oxygen has formal charge -2, the (001) layers in so-called II-IV perovskite oxides (in which the A-site cation is divalent and the B-site cation has formal charge +4) are charge neutral. In III-III perovskite oxides (in which both A- and B-site cations have formal charge +3), the AO layer has charge +1 and the BO₂ layer has charge -1.

As example II-IV ferroelectric materials with charge-neutral layers we choose PbTiO₃ and BaTiO₃; the polar discontinuity at their surfaces (that is their interface with the vacuum), and hence their bound surface charge, derives entirely from their spontaneous polarization. To illustrate the two possible behaviors of centrosymmetric ionic insulators, we choose SrTiO₃, with its neutral layers and zero-containing polarization lattice, and LaAlO₃, whose layers are charged, and whose polarization lattice contains the half quantum. The polar discontinuity between these two materials at their (001) interface has been of particular recent interest [19–21]. The main part of this paper combines the concepts developed for both of these pairs of example materials to treat the case of BiFeO₃, with its combined spontaneous and layer polarizations.

III. SURFACE EFFECTS IN FERROELECTRIC MATERIALS WITH ZERO LAYER POLARIZATION

We begin with a brief review of relevant results for the surface properties of the prototypical II-IV perovskite ferroelectrics, PbTiO₃ and BaTiO₃. In both cases, when the ions have the centrosymmetric arrangement of the high-symmetry reference phase, then the polarization lattice contains zero, and is given by Eqn. 2. Correspondingly, the (001) layers have zero formal charges (Fig. 1). As a result, the only contribution to the \vec{P}_{bulk} of Eqn. 1, and hence to the surface charge, is from the spontaneous polarization. In PbTiO₃ the spontaneous polarization in the ferroelectric phase is oriented along a Cartesian axis ([001] in Fig. 1) and has the value $\sim 80 \mu\text{C cm}^{-2}$; in BaTiO₃ there are a series of phase transitions with the polarization (of magnitude $\sim 25 \mu\text{C cm}^{-2}$) reorienting from the cubic [111] to [011] to [001] directions as the temperature is lowered; we show the low-temperature [001] case in Fig. 1b. The bound surface charge on a (001) surface (Fig. 2) is then given trivially by the component of the spontaneous polarization perpendicular to the surface (80 or $25 \mu\text{C cm}^{-2}$ for PbTiO₃ and BaTiO₃ respectively). It is negative (positive) on the upper surface for downward (upward) pointing polarization, and does not depend on the choice of layer (AO or BO₂) termination. In all cases, the uncompensated (001) surface is electrostatically unstable when the ferroelectric polarization is

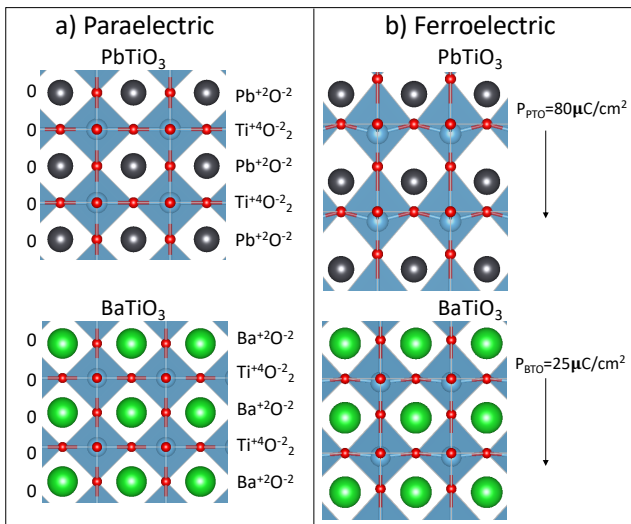


FIG. 1. Crystal structure and (001) layer charges of PbTiO_3 (top) and BaTiO_3 (bottom). a) Arrangement of ions in the high-symmetry centrosymmetric reference structures. On the left of the crystal structure is the total charge for each layer, on the right the composition of each layer. b) Arrangement of ions in the ferroelectric structure. The arrows indicate the direction of the ferroelectric polarization. Pb is in black, Ti in blue, Ba in green and O in red.

along the $[001]$ axis.

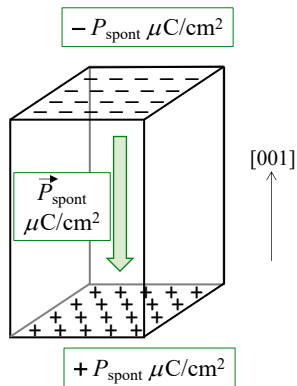


FIG. 2. In ferroelectric materials with uncharged layers, such as BaTiO_3 and PbTiO_3 , the sign and magnitude of the surface charge are determined by the spontaneous polarization, \vec{P}_{spont} .

The electrostatic instability associated with the spontaneous polarization in ferroelectrics is often discussed in terms of a depolarizing field, which acts in the opposite direction to the polarization to suppress the ferroelectricity in thin films. For a film with no compensation from external species, four main responses are known, as sketched in Fig. 3. Polarization reorientation into the plane of the film (Fig. 3a) completely eliminates the

bound surface charge, and so is energetically favorable if it is not prohibited by, for example, strain effects [22]. If in-plane rotation of the polarization is unfavorable, the formation of domains can occur. The example of small domains of opposite orientation [23–25] shown in Fig. 3b reduces the overall charge on each surface; other more exotic textures such as polar skyrmions have also been reported [26–29]. Screening surface charges can in principle be generated by electron-hole excitation across the band gap [1] (Fig. 3c), although, since band gaps are typically of the order of an eV in ferroelectrics this is energetically expensive. Finally, complete suppression of the polarization (Fig. 3d) can occur, usually manifesting as a critical thickness of the paraelectric reference structure before the ferroelectric phase emerges [23, 30, 31].

Screening can also occur from extrinsic factors. When metallic electrodes are present, then carriers from the metal can provide compensating external surface charge to screen the polarization discontinuity. Unless the screening is completely effective, however, the magnitude of the polarization and the ferroelectric Curie temperature, T_c , tend to be reduced from their bulk values [3, 13, 32–34] and there still tends to be a critical thickness below which the paraelectric phase is stable [13, 35]. In the absence of electrodes (or in combination with a bottom electrode), compensating charge can be provided by ions from the environment [8]; this is the physics behind the well-known pyroelectric effect, in which the reduction in polarization on heating releases charged species from the surface [36]. Recently, the reciprocal effect has been demonstrated, in which adsorption of adsorbates carrying a specific charge was shown to switch the ferroelectric polarization to achieve an electrostatically stable surface configuration [4, 8, 11]. Finally, we mention that the presence of charged ions in the growth chamber atmosphere has been exploited to enable growth of single-domain ultra-thin ferroelectric films of PbTiO_3 on SrRuO_3 through metalorganic chemical vapor deposition of PbTiO_3 on SrRuO_3 [2]. A charged atmosphere has even been shown to be more effective in screening the polarization than a top electrode for BaTiO_3 films grown on SrRuO_3 using pulsed laser deposition [10].

IV. SURFACE EFFECTS ARISING FROM THE LAYER-CHARGE POLARIZATION IN NON-FERROELECTRIC MATERIALS

A pair of well-known centrosymmetric materials that illustrate the two cases of “zero-containing” or “half-quantum-containing” polarization lattices are the perovskite-structure oxides strontium titanate, SrTiO_3 , and lanthanum aluminate, LaAlO_3 , shown in Fig. 4. (Note that rotations of the oxygen octahedra, which lower the symmetry from the ideal cubic perovskite structure, occur in both materials; since these rotations preserve the center of inversion they do not change the polar-

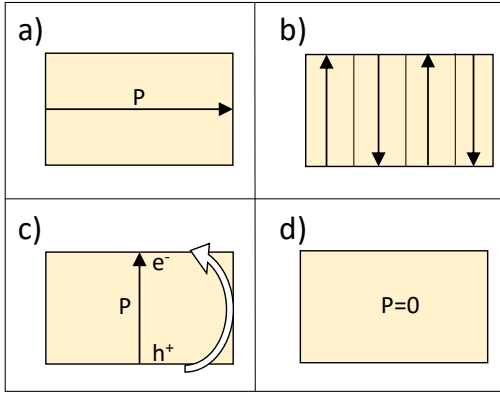


FIG. 3. Effects of the depolarizing field on a ferroelectric thin film. a) In-plane polarization; b) Formation of domains; c) Accumulation of interfacial charge, for example by electron-hole excitation across the gap; d) Phase transition to a non-polar phase.

ization behavior and we do not consider them here.) We discuss next how the different polarization lattice types correspond to their different polarization charges and result in different surface charges, focussing on the (001) surface for conciseness. For a more comprehensive discussion we direct the reader to Ref. 1.

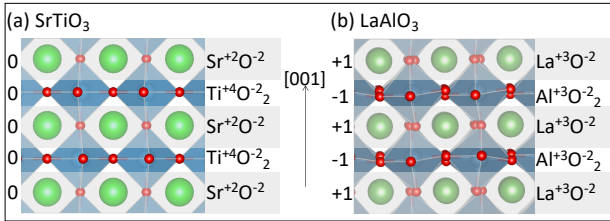


FIG. 4. Crystal structure and (100) layer charges of a) SrTiO₃ and b) LaAlO₃. On the left of the crystal structure is the total charge for each layer, on the right the composition of each layer.

Since SrTiO₃ is a II-IV perovskite, and LaAlO₃ is a III-III perovskite, it is trivial to show, by calculating the polarization as $\vec{P} = \frac{1}{V} \sum_i Z_i \vec{r}_i$, that SrTiO₃ has the zero-containing polarization lattice of Eqn. 2, and LaAlO₃ the half-quantum-containing form of Eqn. 3. Here, Z_i are the formal ionic charges and \vec{r}_i their positions within any choice of unit cell. (Note that rigorous calculation using the Berry phase formalism gives an identical result, and the use of the formal charges when calculating the lattice polarization of the paraelectric structure is formally correct [1].) As a result, the (001) surface of SrTiO₃ has a charge of zero or $n\vec{P}_q$, whereas that of LaAlO₃ has a

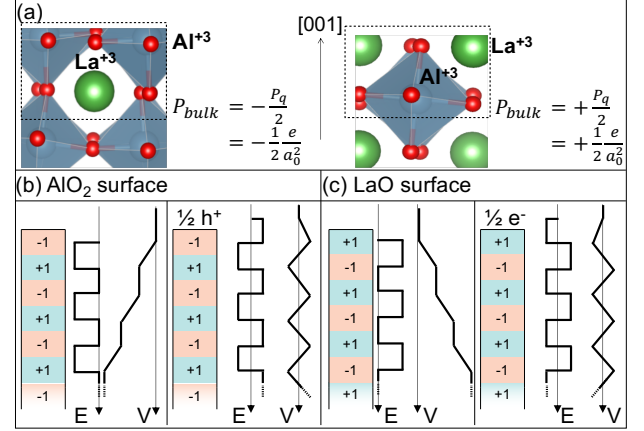


FIG. 5. a) Unit cell of LaAlO₃ with AlO₂ (left) and LaO (right) termination. The dotted-line box indicates the basis used to calculate \vec{P}_{bulk} , and the surface termination is the topmost layer in the box. \vec{P}_{bulk} in the [001] direction is of opposite sign for the two systems. b-c) Electric field E and potential V along the [001] direction for LaAlO₃ with b) AlO₂ and c) LaO termination. The system on the left in each panel has no compensation and so V diverges with thickness. The system on the right has a surface compensation of 1/2 of the layer charge and therefore is stable.

charge of $\frac{n\vec{P}_q}{2}$.

A convenient recipe was provided in Ref. 1 to determine which branch of the polarization lattice (that is, which value of n) is the relevant one for a particular choice of surface plane and chemistry: Take the unit cell that tiles the semi-infinite slab containing the surface of interest, and calculate the dipole per unit volume for that unit cell. The answer is \vec{P}_{bulk} with the appropriate choice of polarization lattice branch. For the (001) surface of SrTiO₃, both smooth surfaces (containing SrO or TiO₂) yield $\vec{P}_{\text{bulk}} = 0$ with this recipe. Therefore they have no bound charge and do not require any external charge compensation. For the (001) surface of LaAlO₃ (Fig. 5a), the LaO surface has [001] polarization value $\vec{P}_{\text{bulk}} = +\frac{1}{2} \frac{|e|}{a_0^2} = +\frac{\vec{P}_q}{2}$, requiring compensation by a negative of charge of this size and the AlO₂ surface has $\vec{P}_{\text{bulk}} = -\frac{1}{2} \frac{|e|}{a_0^2} = -\frac{\vec{P}_q}{2}$, requiring compensation by the corresponding positive charge. (a_0 is the length of the pseudo-cubic unit cell, and the polarization quantum is $\vec{P}_q = \frac{|e|}{a_0^2}$.) The required compensation of half an electronic charge per simple cubic unit cell corresponds to the convenient value of 50 $\mu\text{C cm}^{-2}$ in the conventional units used in the ferroelectrics literature, taking a cubic lattice constant of 4 Å which is slightly larger than the values for SrTiO₃ (~ 3.9 Å) and LaAlO₃ (~ 3.8 Å).

An alternative picture that is intuitively appealing, although not as rigorously well-founded, is to decompose the materials into planes of ions and consider the net charges of these planes, as shown in Fig. 4. For the case of II-IV perovskites such as SrTiO_3 , the (001) planes are alternately SrO and TiO_2 , both of which are charge neutral. Therefore any planar (001) surface in a II-IV perovskite carries no net surface charge and so is stable. In III-III perovskites such as LaAlO_3 , the (001) planes are alternately LaO and AlO_2 with charges $+1 e$ and $-1 e$ per unit cell respectively. And so, depending on the choice of termination, the surface has the corresponding positive or negative charge per surface unit cell, that is $\pm 100 \mu\text{C cm}^{-2}$. As illustrated in Fig. 5b, the positive layer charge of the LaO surface requires a compensating negative charge of *half* the layer charge, that is $-0.5 e$ per unit cell or $-50 \mu\text{C cm}^{-2}$, to prevent a divergence of the electrostatic potential and stabilize the surface. (A compensating charge *equal* to the surface charge just displaces the problem to a new terminating layer [37].) Likewise, the formally negatively charged AlO_2 surface (Fig. 5c) requires a compensating positive charge of the same amount. Thus we reach the same conclusion as that derived from consideration of the bulk polarization.

The implication of the different bulk polarization lattices of LaAlO_3 and SrTiO_3 for the *interface* between the two materials is profound: The polarization discontinuity between the two materials means that it is not possible to make a stoichiometric interface that is electrostatically stable [38]. Specifically, an $\text{SrO} / \text{AlO}_2$ interface requires a compensating positive charge of magnitude half an electronic charge per unit cell, and the $\text{LaO} / \text{TiO}_2$ interface requires half an electronic charge per unit cell of negative charge. In the latter case, the extra electrons occupy the broad Ti $3d$ -derived energy bands at the bottom of the valence band. The compensating electrons are therefore mobile and form an interfacial two-dimensional electron gas [19], a remarkable behavior for the interface of two robust band insulators. The electron gas has even been shown to be superconducting at low temperature [21].

Note that these considerations are not limited to III-III perovskites, but are relevant for the surfaces and interfaces of all centrosymmetric insulators that have a “half-quantum containing” polarization lattice. Another example is provided by the I-V perovskites, such as KTaO_3 , where surface reconstructions [9] and surface and interface 2D electron gases [39, 40] have been observed.

V. SURFACES OF FERROELECTRIC MATERIALS WITH CHARGED LAYERS – THE INTERPLAY OF LAYER CHARGE AND SPONTANEOUS POLARIZATION IN BISMUTH FERRITE

Next we turn to the case of ferroelectric materials whose polarization lattice in their high-symmetry centrosymmetric prototype structure contains the half-

polarization quantum. We choose the example of the III-III ferroelectric perovskite BiFeO_3 , which, as mentioned in the introduction, combines a half-quantum-containing polarization lattice in its centrosymmetric reference structure, with a spontaneous polarization of almost exactly $50 \mu\text{C cm}^{-2}$ in the [001] direction. In particular, we will explore the consequences of the accidental layer- and spontaneous polarization-surface charge compensation on the stability of thin films and heterostructures of BiFeO_3 .

The ground state of bulk BiFeO_3 has the $R3c$ structure, which is reached from the prototypical cubic perovskite structure by alternating rotations of the oxygen octahedra around the [111] axis, combined with opposite displacements of anions and cations along the [111] direction. The latter results in a large spontaneous polarization of magnitude $\sim 90 \mu\text{C cm}^{-2}$ oriented along [111]. In Fig. 6 we show the evolution of the polarization (calculated using the Berry phase approach in Ref. 41) as a function of the amplitude of the ferroelectric distortion from the high-symmetry reference structure (0% distortion) to the ground-state ferroelectric structure (100% distortion), for several branches of the polarization lattice. The spontaneous ferroelectric polarization along [111] is highlighted in red. Interestingly, and completely coincidentally, the value of the spontaneous polarization is very close to half of the polarization quantum of $\sim 180 \mu\text{C cm}^{-2}$ along the [111] direction (highlighted in blue in Fig. 6) for BiFeO_3 . Since the polarization lattice for the centrosymmetric reference structure is of the half-quantum type, we see that there are two combinations of the centrosymmetric layer polarization and the spontaneous polarization ($+\frac{\vec{P}_q}{2}$ with $P_{\text{spont}} = -90 \mu\text{C cm}^{-2}$, and $-\frac{\vec{P}_q}{2}$ with $P_{\text{spont}} = +90 \mu\text{C cm}^{-2}$) that combine to give a bulk polarization value, \vec{P}_{bulk} , in the ferroelectric structure that is very close to zero (in fact $\pm 2.3 \mu\text{C cm}^{-2}$ in Fig. 6).

This in turn leads to a cancellation of the bound surface charge, $\sigma_{\text{surf}} \approx 0$. A consequence of this cancellation, therefore, is that free-standing thin films of BiFeO_3 are electrostatically stable for one choice of polarization for each surface; this has been referred to as the “happy” configuration in the literature [42].

In Fig. 7 we illustrate this with a cartoon of a free-standing BiFeO_3 slab in the commonly grown [001] orientation. The projection of the [111]-oriented ferroelectric polarization into the [001] direction results in a spontaneous [001] polarization of $\sim \pm 50 \mu\text{C cm}^{-2}$. As we saw in the case of LaAlO_3 in Section IV, the unit cell corresponding to the BO_2 (FeO_2 in this case) surface selects for the branch on the centrosymmetric polarization lattice with value $-\frac{1}{2} \frac{e}{a_0^2} = -50 \mu\text{C cm}^{-2}$. Therefore an FeO_2 surface with a positive (i.e. pointing towards it, or upwards in Fig. 7a) value of spontaneous polarization has zero surface charge and is stable; conversely the AO (BiO in this case) surface selects for the $+\frac{1}{2} \frac{e}{a_0^2} = +50 \mu\text{C cm}^{-2}$ half quantum, and requires a negative (i.e. point-

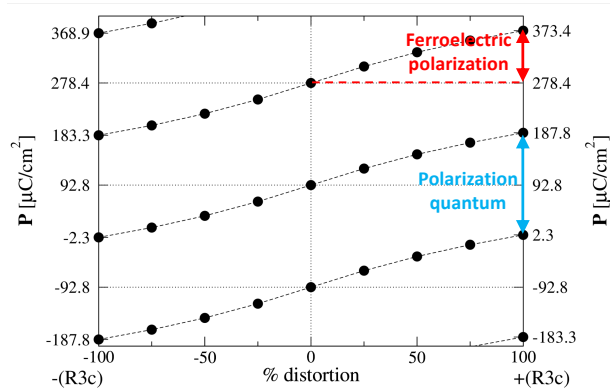


FIG. 6. Polarization in the [111] direction for BiFeO_3 , calculated using the LSDA+ U and Berry phase methods within density functional theory in Ref. 41. $\pm 100\%$ distortion corresponds to the ground-state $R3c$ structures of opposite polarization; 0% distortion corresponds to the ideal cubic perovskite structure. Three full branches of the polarization lattice are shown. The central branch illustrates that, starting from a centrosymmetric polarization of $92.8 \mu\text{C cm}^{-2}$ ($= \frac{P_q}{2}$) and introducing a negative spontaneous polarization yields a bulk polarization close to zero (in fact $-2.3 \mu\text{C cm}^{-2}$) and a correspondingly small surface charge. Introducing a positive spontaneous polarization in this branch results in a very large bulk polarization ($187.8 \mu\text{C cm}^{-2}$) and an unfavorably large surface charge. The lower branch illustrates the opposite scenario. Reproduced from Ref. 41. Copyright 2005 by the American Physical Society.

ing away from it) polarization to ensure stability. Note that the opposite combinations are twice as unfavorable (“unhappy”) as they would be in a II-IV perovskite with the same magnitude of spontaneous polarization but uncharged layers (Fig. 7b), since they would have a surface charge of $\pm 100 \mu\text{C cm}^{-2}$. In the alternative charged-layers picture, the centrosymmetric BiFeO_3 is composed of alternating (001) layers of positively charged BiO ($+1 e$ per unit cell or $\sim +100 \mu\text{C cm}^{-2}$) and negatively charged FeO_2 ($-1 e$ per unit cell or $\sim -100 \mu\text{C cm}^{-2}$). The appropriately oriented spontaneous polarization of magnitude $50 \mu\text{C cm}^{-2}$ then provides the required compensating surface charge of half that amount.

Next, we discuss the consequences of this layer and spontaneous polarization cancellation, examining examples from the literature as well as presenting new results of behaviors that are caused by the happiness or unhappiness of BiFeO_3 surfaces and interfaces. We consider three scenarios: first, BiFeO_3 on a metallic substrate, followed by interfaces with centrosymmetric II-IV then III-III insulators.

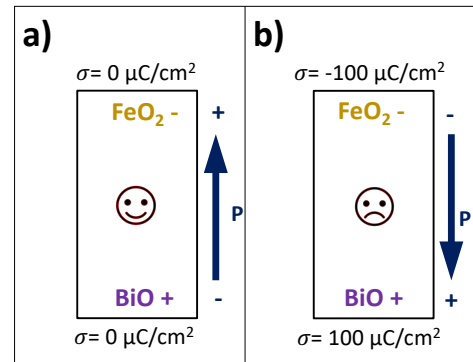


FIG. 7. Combinations of ferroelectric polarization direction and surface termination leading to a) stable (happy) and b) unstable (unhappy) BiFeO_3 (001) surfaces. In a), the spontaneous polarization, $P_{\text{spont}} = 50 \mu\text{C cm}^{-2}$ is compensated by the layer polarization. In b) the layer polarization adds to the spontaneous polarization $P_{\text{spont}} = -50 \mu\text{C cm}^{-2}$ to give a surface charge of $\pm 100 \mu\text{C cm}^{-2}$.

A. Interaction of BiFeO_3 thin films with a metal substrate

We begin with the case of BiFeO_3 films grown on substrates that are metallic, and therefore provide good screening of any interfacial charge at the bottom interface. We expect, therefore, that the orientation of the spontaneous polarization will be determined by the nature of the top surface with the vacuum.

We take the examples of BiFeO_3 on two metallic oxides, $\text{La}_{0.7}\text{Sr}_{0.3}\text{MnO}_3$ (LSMO) and SrRuO_3 . Heterostructures of these combinations were grown and characterized in Ref. 43, and we begin by analyzing the results of that work in the context of the surface electrostatics introduced above.

In Ref. 43, the SrRuO_3 substrate was terminated with an SrO layer, and so the bismuth ferrite film, which grows in complete BiFeO_3 unit cells, began with an FeO_2 layer and ended with a BiO surface. As expected, the polarization spontaneously adopted the down orientation, corresponding to zero surface charge. An FeO_2 surface was achieved for BiFeO_3 on SrRuO_3 by inserting a monolayer of TiO_2 at the interface so that the BiFeO_3 film began with a BiO layer. This caused a spontaneous upwards polarization in the BiFeO_3 , again corresponding to the zero surface-charge configuration as expected.

Growth of BiFeO_3 on LSMO shows a similar behavior. In Fig. 8 we show two high-angle annular dark-field scanning transmission electron microscopy (HAADF-STEM) images of the BiFeO_3 on LSMO heterostructures grown in Ref. 43. (For additional details about the thin film growth see section VII and Ref. 43.) In panel a the LSMO is terminated with MnO_2 , so the BiFeO_3 layer has an FeO_2 surface, while in panel b the LSMO is (La,Sr)O

terminated, so the bismuth ferrite starts with a FeO_2 layer and has a BiO surface. We have overlaid arrows, which are vector maps indicating the local polarization extracted from the measured atomic positions, in the BiFeO_3 layers. Again, as expected from the surface electrostatics, we see that case (a) develops a spontaneous up-pointing polarization (\vec{P} pointing towards the FeO_2 surface) and case (b) a spontaneous down-pointing (\vec{P} pointing away from the BiO surface). In all four scenarios switching of the polarization was achieved using a tip in a piezoforce geometry, but with considerable exchange bias favoring the spontaneous orientation.

In our discussion so far, we have assumed that the LSMO and SrRuO_3 substrates behave like ideal metals, and have disregarded the fact that their constituent ions have different formal layer charges ($\pm \sim 0.7 e$ for LSMO at 0.3 Sr concentration, and neutral for SrRuO_3). The different formal layer charge discontinuities could play a role if the metallic screening is incomplete. Indeed, it is known that ionic relaxation is an important contributor to surface-charge screening in oxide electrodes [44], and the use of polar metals as electrodes has been proposed as a route to overcoming the critical thickness in ferroelectric capacitors [35]. To investigate the role of the formal layer charges in metallic oxide electrodes, we next perform density functional calculations of [001]-oriented $\text{BiFeO}_3/\text{SrRuO}_3$ superlattices in both the happy (Fig. 7a) and sad (Fig. 7b) interfacial orientations (for details see the methods in Section VII).

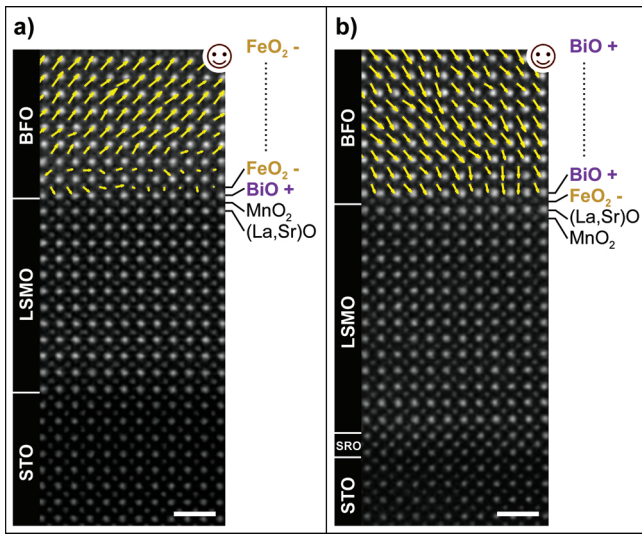


FIG. 8. Cross-sectional HAADF-STEM images of two distinct $\text{BiFeO}_3/\text{La}_{0.7}\text{Sr}_{0.3}\text{MnO}_3$ heterointerfaces with overlaid vector maps showing the polarization in the BiFeO_3 layers. a) The sample with the MnO_2 -terminated ($\text{La}_{0.7}\text{Sr}_{0.3}\text{O}-\text{MnO}_2-\text{BiO}-\text{FeO}_2$) interface develops a spontaneous up-pointing polarization (\vec{P} pointing towards the FeO_2 surface). b) The sample with the $\text{La}_{0.7}\text{Sr}_{0.3}\text{O}$ -terminated ($\text{MnO}_2-\text{La}_{0.7}\text{Sr}_{0.3}\text{O}-\text{FeO}_2-\text{BiO}$) interface develops a spontaneous down-pointing polarization (\vec{P} pointing away the BiO surface). The scale bar is 1 nm.

We constructed two superlattices each containing six layers of BiFeO_3 and four layers of SrRuO_3 , with one SrO/FeO_2 and one BiO/RuO_2 interface, see Fig. 9. The two supercells had opposite orientation of the BiFeO_3 ferroelectric polarization, such that one system had self-compensating (Fig. 9a) and the other charged interfaces (Fig. 9b). In both cases, the entire heterostructure adopts the $a^-a^-c^-$ tilt pattern of BiFeO_3 (Fig. 9, left panels), and both materials maintain their bulk magnetic orderings (G-type antiferromagnetic for BiFeO_3 and ferromagnetic for SrRuO_3). As expected, both from our electrostatic arguments and from the experimentally observed exchange bias [43], the happy system is energetically the most stable, $\sim 2 eV$ per supercell lower in energy than the unhappy system.

The calculated structures, layer-by-layer polarizations and layer-resolved densities of states are shown in Fig. 9. Note that, in both the “happy” and “unhappy” systems, the SrRuO_3 layers are metallic (in green in the density of states graph on the right-hand-side on Fig. 9), with a finite density of states at the Fermi energy in all layers, and the BiFeO_3 (in purple) is insulating, with the Fermi energy (shown as a vertical red line) lying in the gap. The layer-resolved densities of states for the happy system (right-most panel of Fig. 9a) indicate that there is no band bending and hence no internal electric field in the happy system, consistent with the absence of surface charge in the happy BiFeO_3 slabs. The polarization (middle panel) has its full bulk value throughout the slab, and drops abruptly to zero in the first layer of the SrRuO_3 .

For the six-unit-cell BiFeO_3 heterostructures that we present here, we find that the unhappy system is metastable in our DFT calculations. (For thinner films the polarization orientation reverses and the structure relaxes to the happy system.) We find, however, a suppressed layer polarization compared with the happy system, as visible in the middle graph of Fig. 9b, as well as a pronounced shift in the BiFeO_3 band edges from layer to layer indicating a strong internal electric field resulting from the large uncompensated surface charges in the BiFeO_3 slab. In addition, the interfacial SrRuO_3 layers undergo a polar ionic distortion to further reduce the polar discontinuity, similar to that observed in Ref. 35 for the $\text{SrRuO}_3/\text{BaTiO}_3$ interface.

In summary, our calculations indicate that, even with metallic screening, the direction of polarization preferred by the interplay between the lattice and spontaneous polarization of the ferroelectric layer is strongly preferred. While screening by the metal is able to stabilize the unhappy polarization orientation it is still energetically unfavorable. This behavior explains the strong electric-field exchange bias effects [45], as well as the highly asymmetric resistive switching [46] found in BiFeO_3 capacitors.

As a final example from the literature, we choose the case of heterostructures between BiFeO_3 and the metallic lightly-doped II-IV magnetic insulator, CaMnO_3 . Heterostructures of $\text{Ca}_{1-x}\text{Ce}_x\text{MnO}_3/\text{BiFeO}_3$ were grown on YAlO_3 , whose small lattice constant causes a strongly

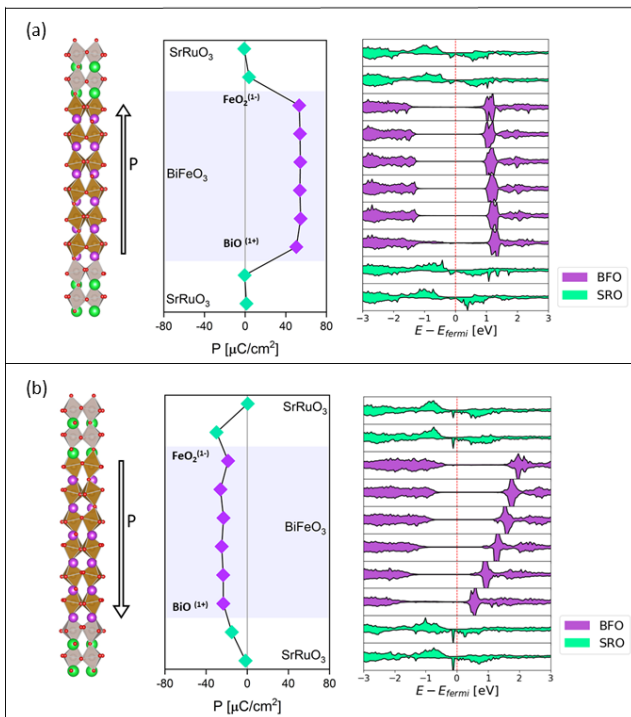


FIG. 9. Calculated structures (left), layer by layer polarizations (middle) and layer density of states (right) for the two $\text{BiFeO}_3/\text{SrRuO}_3$ heterostructures studied in this work. Panel a) shows the happy BiFeO_3 slab configuration; panel b) the unhappy. Green symbols and shading indicate SrRuO_3 ; BiFeO_3 is shown in purple.

compressive biaxial in-plane strain and correspondingly large out-of-plane lattice constant and polarization (see detailed discussion in Subsection C) [47]. The ferroelectric polarization was determined to have an out-of-plane value of $\sim 100 \mu\text{C}/\text{cm}^2$, and to point towards the $\text{BiFeO}_3/\text{CaMnO}_3$ interface, which was of the $\text{FeO}_2^- - \text{CaO}$ type. While this is the least unhappy arrangement, in this case, because of the unusually large out-of-plane polarization, the FeO_2^- layer provides only partial compensation of the bound surface charge. An additional electronic charge accumulation of ~ 0.65 electrons per unit cell area was found using electron energy loss spectroscopy (EELS) to accumulate in the near-interfacial $\text{Ca}_{1-x}\text{Ce}_x\text{MnO}_3$ layers.

B. Interfaces of bismuth ferrite with centrosymmetric II/IV insulating perovskites

Since the (100) surface of a centrosymmetric II/IV insulating perovskite such as SrTiO_3 has zero bound charge, we expect it to behave electrostatically similarly to the vacuum in its interface with BiFeO_3 . That is, we expect that BiFeO_3 surfaces that are happy in free-standing slabs to form stable interfaces with SrTiO_3 , with bulk-like ferroelectricity in the BiFeO_3 layer down

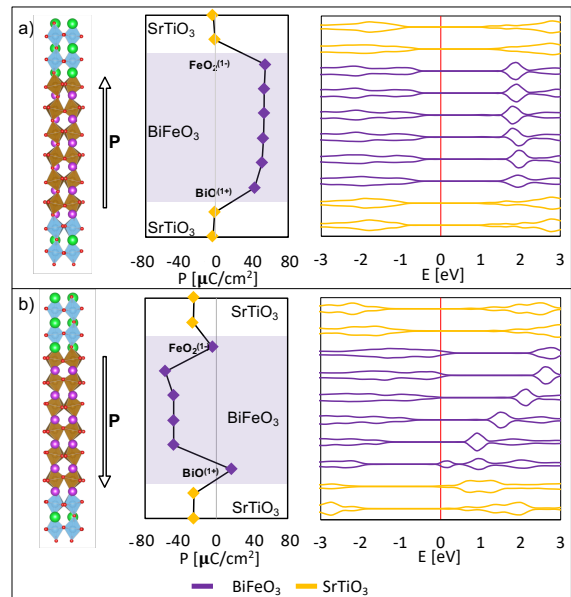


FIG. 10. Polarization along the [001] direction of a $(\text{SrTiO}_3)_4/(\text{BiFeO}_3)_6$ heterostructure with one BiO/TiO_2 interface and one FeO_2/SrO interface. The polarization direction leading to a happy system is in panel a, and to an unhappy system in panel b. The systems are shown on the left, in the middle their corresponding unit cell-by-unit cell polarization and on the right the unit cell-by-unit cell local density of states. Orange data points correspond to SrTiO_3 and purple ones to BiFeO_3 . In the atomic structure Sr is green, Ti blue, Bi purple, Fe brown and O red.

to small thicknesses, whereas electrostatically unstable surfaces will have similarly unhappy interfaces with SrTiO_3 and their ferroelectric polarization will tend to reverse [42]. All the examples that we have been able to find of experimental $\text{BiFeO}_3/\text{SrTiO}_3$ superlattices and heterostructures have their as-grown polarization orientation in the direction which compensates the layer polarization, consistent with this assumption [48–51]. Likewise, literature calculations of $\text{PbTiO}_3/\text{BiFeO}_3$ superlattices, with the polarization of the PbTiO_3 entirely in the plane of the superlattice [52], found a stable solution with BiFeO_3 in its happy configuration.

To explore the details of the behavior, we perform DFT calculations for two [001] superlattices, each containing four layers of SrTiO_3 and six layers of BiFeO_3 with one SrO/FeO_2 and one BiO/TiO_2 interface, but with the BiFeO_3 polarization initialized to opposite orientations. As expected, we find that the happy case is stable, with the layer polarization close to the bulk value throughout the film (Fig. 10a, middle panel). As in the case of the interface with SrRuO_3 , the unit cell-by-unit cell density of states indicates zero internal electric field in ferroelectric BiFeO_3 since the charge compensation between the spontaneous and layer polarization leads to zero surface charge. In contrast, we are unable to stabilize the un-

happy state in our DFT calculations unless we constrain the polarization orientation in the middle layers of the BiFeO₃ slab (Fig. 10b). The layer-by-layer density of states indicates a strong band bending due to the large internal electric field, and the formation of metallic layers by electron-hole excitation across the band gap at the interfaces. (Similar metallicity at the unhappy BiO / TiO₂ interface was seen in an earlier DFT calculation for a non-stoichiometric BiFeO₃ slab with both of its interfaces set to BiO sandwiched between two SrTiO₃ layers [53].) Additionally, the SrTiO₃, which is an incipient ferroelectric and therefore readily polarizable, develops a polarization parallel to the spontaneous polarization of BiFeO₃ to reduce the polar discontinuity.

C. Interfaces of bismuth ferrite with insulating centrosymmetric III-III perovskites

Finally, we consider the case of the interface between BiFeO₃ and a centrosymmetric insulating III-III perovskite, which contains $\frac{\vec{P}_g}{2}$ in its polarization lattice. Here the centrosymmetric contributions to the polarization lattice are similar in both materials (they will differ slightly if the lattice vectors and unit cell volumes are different) and so the interfacial polar discontinuity is given by the difference in spontaneous polarizations. If the second material is centrosymmetric, then the polar discontinuity is equal to the spontaneous polarization of BiFeO₃, similar to the case of the interfaces between the II-IV ferroelectrics PbTiO₃ or BaTiO₃ and vacuum discussed above.

A number of different routes to avoiding the polarization discontinuity at the interface, of the types we summarized in Fig. 3, have been observed. An in-plane polarization (Fig. 3a) associated with an orthorhombic phase has been reported for BiFeO₃ on a NdScO₃ substrate, which also imparts a small biaxial tensile strain [54]. Since many low-energy metastable non-polar, antipolar and even antiferroelectric phases of BiFeO₃ are known [55, 56], the BiFeO₃ film can also lose its polarization entirely (Fig. 3d). For example, in superlattices and heterostructures of BiFeO₃ with centrosymmetric *Pnma* LaFeO₃, BiFeO₃ has been reported to adopt the antiferroelectric PbZrO₃ structure [57, 58], or even observed in an entirely new antiferroelectric structure, which has not been reported in the bulk [15]. Density functional calculations indicated that, for the strain conditions of the sample, this antiferroelectric phase is only slightly higher in energy than the ground-state polar phase, and it is favored because of its lower electrostatic energy cost [15]. (Note that a DFT calculation for a BiFeO₃/LaFeO₃ slab in vacuum suggested the formation of a metallic layer at the interface, although that study did not explore the formation of non-polar BiFeO₃ phases and it is unclear how the polar discontinuities at the surface were treated in the calculation [59].)

Another route to the compensation of the polar dis-

continuity is the creation of extended defects; we discuss the example of LaAlO₃/BiFeO₃, where this behavior has been observed, next. Under strong biaxial compressive strain, imposed by a small-lattice-constant substrate such as LaAlO₃, BiFeO₃ is known to undergo a phase transition to a tetragonal or tetragonal-like phase (T-BiFeO₃) with a large *c/a* ratio of ~ 1.3 and a giant, almost entirely out-of-plane spontaneous polarization of $\sim 150 \mu\text{C cm}^{-2}$ [60–62]. This spontaneous polarization is roughly three times the [001] spontaneous polarization of the usual rhombohedral phase of BiFeO₃, and correspondingly roughly three times the half-polarization quantum. (Note that the half-polarization quantum for T-BiFeO₃ is slightly larger, at $59 \mu\text{C/cm}^2$, than that of the usual rhombohedral phase, because of its different lattice parameters. We obtain values of $a = b = 3.67 \text{ \AA}$ and $c = 4.64 \text{ \AA}$ in our calculations for the lowest energy tetragonal structure.) This giant spontaneous polarization has two implications: First, the spontaneous polarization can be at best only partially compensated by the layer polarization at a flat and stoichiometric BiO or FeO₂ (001) surface. Second, the giant polarization means that the electrostatic potential diverges strongly at an interface, and only a few layers can form before a compensation mechanism is required. In Fig. 11 we show a HAADF-STEM image of a 100nm-thick film of T-BiFeO₃ on LaAlO₃, in which, we observe such a compensation mechanism in the formation of an extended planar defect just a few unit cells above the T-BiFeO₃/LaAlO₃ interface. We indicate the local ferroelectric polarization (plotted opposite to the atomic displacements of the Fe cations) by the yellow arrows in Fig. 11; this vector map reveals that the first five to seven T-BiFeO₃ unit cells above the T-BiFeO₃/LaAlO₃ interface develop a spontaneous up-pointing polarization. Then, perhaps unexpectedly, above the extended planar defect the polarization in the T-BiFeO₃ lattice is reversed and a down-pointing polarization forms. This results in a head-to-head polarization configuration, with a giant discontinuity of the *spontaneous* polarization of $\sim 300 \mu\text{C cm}^{-2}$. For both the top and bottom layers, however, the stoichiometric BiFeO₃ terminates with an FeO₂ layer, so the absolute polarization of each layer is reduced from the spontaneous polarization by half a quantum, to $\sim 100 \mu\text{C cm}^{-2}$. Note that this is the “happiest” configuration possible for T-BiFeO₃, which, we emphasize again, does not have the accidental cancellation between its spontaneous polarization and the half-polarization quantum seen in the rhombohedral ground state. Correspondingly, the *absolute* polar discontinuity between the two T-BiFeO₃ layers is reduced to the (still very large!) value of $\sim 200 \mu\text{C cm}^{-2}$.

The planar defect (highlighted with red rectangles in Fig. 11) consists of a characteristic Bi₂O₂²⁺ layer, which shifts the perovskite layers above the defect half a perovskite block along the orthogonal horizontal directions in the manner of an Aurivillius phase, surrounded by two O²⁻ layers (see cartoon on the right side of Fig. 11; the

horizontal red lines indicate the boundary of the defect). The total stoichiometry of the defect consists of one formally $\text{Bi}_2\text{O}_2^{2+}$ block plus two O^{2-} ions per surface BiFeO_3 unit cell, leading to a net defect charge of two electrons, or $\sim -100\mu\text{C cm}^{-2}$, per primitive unit cell cross-sectional area. This is exactly half of the polar discontinuity, and so, as sketched in the lower panel of Fig. 5, is exactly the layer charge needed for compensation. Note that oxygen non-stoichiometry in the Aurivillius-like layer, yielding $\text{Bi}_2\text{O}_{2\pm\delta}$ rather than precisely Bi_2O_2 , is likely, and will change the exact amount of compensating charge that it provides. Indeed, a similar planar defect, with a *double* $\text{Bi}_2\text{O}_2^{2+}$ layer, was observed in a BiFeO_3 film grown on an LaAlO_3 substrate in spite of an intermediate metallic electrode between the film and the substrate [63]. In this case the BiFeO_3 layer adjacent to the electrode was non-polar, and that above the defect developed a downward-pointing polarization as in our example.

Interestingly, a similar extended defect has been reported as a surface “skin” in BiFeO_3 , in all cases when the polarization points in the upwards (towards the surface) direction [64–66]. In Ref. 65 a film of rhombohedral BiFeO_3 was grown in [001] orientation on an insulating DyScO_3 substrate, and two opposite domains, separated by a 180° domain wall were imaged using HAADF-STEM. The down-polarization domain had a pristine BiO surface and so was in the ‘happy’ configuration. The up-polarization domain, which would have been in the ‘unhappy’ configuration with an excess positive charge in its pristine form, had a capping layer of the negatively-charged Bi_2O_2 Aurivillius-type extended defect to compensate. This finding has clearly unfavourable implications for the switching of BiFeO_3 domains. In Ref. 66, the BiFeO_3 film on TbScO_3 had domains of strongly suppressed polarization alternating with domains of enhanced upward-pointing polarization; the latter had the surface skin overlayer. Finally, we mention that similar Aurivillius structures have also previously been observed as intergrowths in rhombohedral BiFeO_3 thin films [67]. It would be interesting to analyze the interfaces between the intergrowths and the surrounding BiFeO_3 regions to determine the nature of the interface chemistry and the polarization orientation in the context of the compensation principles discussed here.

VI. SUMMARY AND OUTLOOK

In summary, we have reviewed how the spontaneous polarization associated with ferroelectricity combines with the layer polarization associated with the ionic charges of the lattice to determine the electrostatic stability of the surfaces and interfaces of insulators. We reminded the reader that the two contributions are conveniently treated on the same footing by the modern theory of polarization, allowing straightforward determination of the amount of bound charge at a general surface or interface. The bound charge is important for the de-

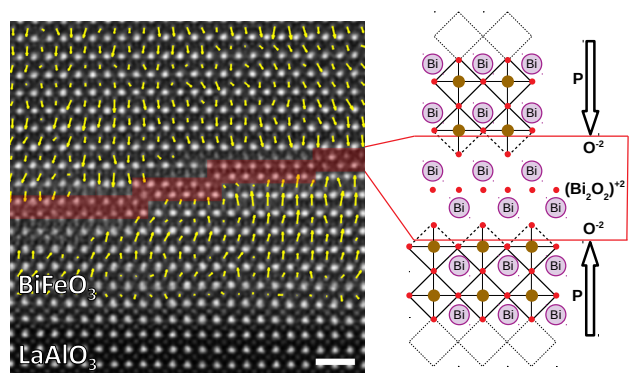


FIG. 11. Cross-sectional HAADF-STEM image showing the presence of planar defects just above the $\text{BiFeO}_3/\text{LaAlO}_3$ interface. The stepped Bi_2O_2 structural units are highlighted by the red rectangles and the overlaid vector map of the ferroelectric polarization plotted opposite to the displacement of the Fe cations (yellow arrows) reveals that the polarization in the pseudo-tetragonal BiFeO_3 lattice changes from up to down direction across the defect. An atomic model of the defect is shown on the right. The scale bar is 1 nm.

sign of thin-film heterostructures and for the stability of surfaces, since any non-zero surface or interfacial charge must be compensated to avoid divergence of the electrostatic potential.

After briefly discussing examples of materials with a spontaneous polarization but no layer polarization ([001]-oriented PbTiO_3 and BaTiO_3) and a material with no spontaneous polarization but a non-zero layer polarization ([001]-oriented LaAlO_3) we focused on the case of multiferroic BiFeO_3 , which combines both spontaneous and layer contributions. BiFeO_3 is of particular interest, because the spontaneous and layer contributions to the polarization in the ground-state $R3c$ structure have the same size along the usual [001] growth direction, leading to combinations of polarization and surface termination that are uncharged and therefore electrostatically stable. The opposite combinations have double the surface charge of a ferroelectric with the same spontaneous polarization but with uncharged layers. These have been referred to as the happy and unhappy combinations in earlier work [42].

We considered three scenarios: BiFeO_3 on a metallic substrate, BiFeO_3 in a superlattice or heterostructure with a zero-layer-charge insulator, and finally a BiFeO_3 /insulator superlattice or heterostructure in which the insulator has the same layer charges as the BiFeO_3 . In each case we illustrated the different possible behaviors with examples from the literature, as well as with density functional calculations and HAADF-STEM analyses performed for this work.

We can summarize the differences in behavior in the three cases as follows: i) Both the happy and the unhappy polarization orientations can be stabilized by a metallic electrode, although the unhappy case is higher in energy

and has a lower spontaneous polarization. This is consistent with the known large electric-field exchange bias of BiFeO₃ films, and implies that symmetric switching of a BiFeO₃ capacitor will be difficult to achieve. ii) The interface of BiFeO₃ with a zero-charge-layer insulator behaves like a free BiFeO₃ surface, with the happy combination of polarization and surface termination strongly favored. The unhappy combination can be stabilized by strong band bending to generate metallic layers at the interface and/or polarization of the adjacent insulator. iii) The interface of BiFeO₃ with another III-III perovskite has a polar discontinuity equal to the spontaneous polarization, and so is equally energetically unfavorable for both orientations of the polarization. As a result of the rich Bi-Fe-O low energy phase space, many responses are possible, including stabilization of phases with zero out-of-plane polarization, and the formation of extended planar defects.

While the electrostatic concepts discussed in this paper are not new, we hope that their collection in this article will be helpful in guiding the design of BiFeO₃ and related thin films or heterostructures with targeted electrical properties, as well as in interpreting experimental observations.

VII. METHODS

Density functional Theory. Density functional calculations were performed within the periodic supercell approach using the VASP code [68–71]. We chose the PBEsol functional [72] for all calculations because i) it gives a good band alignment between metallic SrRuO₃ and BiFeO₃ and no pathological situation arises [73], and ii) it yields a paraelectric ground state for SrTiO₃. In order to obtain a band gap for BiFeO₃ close to the experimental value the Hubbard U , in the Dudarev [74] approach, was used with $U - J = 4$ eV on the Fe 3d states, and $U - J = 2.0$ eV on the Ti and Ru d states. Core electrons were replaced by projector augmented wave (PAW) potentials [75], while the valence states ($5e^-$ for Bi, $8e^-$ for Fe, $6e^-$ for O, $10e^-$ for Sr, $4e^-$ for Ti, $8e^-$ for Ru) were expanded in plane waves with a cut-off energy of 500 eV. In all calculations the in-plane lattice parameters were set to that of SrTiO₃, $a_{\text{PBEsol}} = 3.90$ Å, as it is the substrate commonly used in epitaxial growth of BiFeO₃ thin films. The in-plane surface area is $\sqrt{2}a \times \sqrt{2}a$. A Monkhorst-Pack k -point grid of $(5 \times 5 \times 1)$ was used for all ionic relaxations, which had an optimization threshold on the forces of 0.01 eV/Å. For the density of states calculations, Monkhorst-Pack k -point grid of $11 \times 11 \times 1$ was used. An antiferromagnetic G-type ordering was imposed in BiFeO₃, which gave a magnetic moment of 4.15 μ_B per Fe ion in the bulk. SrRuO₃ instead is ferromagnetic and the magnetic moment is 1.4 μ_B per Ru ion in the bulk.

The unit cell-by-unit cell polarization along the [001] direction shown in Fig. 9 and 10 was calculated by com-

puting the displacement of each ion from the high symmetry position and multiplying it by the Born effective charges from Ref. [41].

Thin Film Growth. The BiFeO₃/La_{0.7}Sr_{0.3}MnO₃ (BFO/LSMO) heterostructures shown in Fig. 8 were grown by pulsed laser deposition on SrTiO₃ (001) (STO) single crystal substrates. Before the growth, a buffered HF acid-etch and thermal treatment process was used to obtain fully TiO₂-terminated surfaces. The sample with the MnO₂-terminated (La_{0.7}Sr_{0.3}O-MnO₂-BiO-FeO₂) interface was designed by growing whole LSMO unit cells directly on the STO substrate, followed by the growth of the BFO layer. For the sample with the La_{0.7}Sr_{0.3}O-terminated (MnO₂-La_{0.7}Sr_{0.3}O-FeO₂-BiO) interface, 1.5 unit cells of SrRuO₃ (SRO) were deposited on STO to switch the termination of the STO from TiO₂ to SrO. The SRO layer was grown at 650 °C in 100 mTorr of oxygen pressure. Both the LSMO and BFO layers were grown at 690 °C in 150 mTorr of oxygen pressure. A postannealing process was carried out at 400 °C under an oxygen ambient for 1 h to ensure the samples were fully oxidized. For additional information, see Ref. [43]. The BFO thin film shown in Fig. 11 was grown by molecular beam epitaxy (MBE) on single-crystal substrates of (001) LaAlO₃ (LAO). The studied 100-nm-thick film showed the coexistence of two interspersed BFO phases: a rhombohedral-like (R) phase and a tetragonal-like (T) phase. Further growth and characterization details can be found in Ref. [60].

Transmission Electron Microscopy. Cross-sectional specimens for transmission electron microscopy analysis were prepared by mechanical polishing using a tripod polisher followed by argon ion milling until electron transparency. High-angle annular dark-field scanning transmission electron microscopy (HAADF-STEM) was carried out using the TEAM 0.5 microscope located at the National Center for Electron Microscopy (NCEM). The TEAM 0.5 is a FEI Titan 80-300 microscope equipped with a high-brightness Schottky-field emission X-FEG electron source, a source monochromator, a CEOS DCOR spherical-aberration probe corrector, and a CEOS CETCOR spherical-aberration image corrector. The microscope was operated at 300 kV, the probe semi-convergence angle set to 16.5 mrad (which yields a calculated probe size of 0.63 Å), and the annular semi-detection range of the HAADF detector calibrated at 45–290 mrad. This setting was chosen to allow for a sufficiently large depth of field in order to enhance the contrast of the atomic columns. The positions of the atomic columns were first fitted by means of a center of mass peak-finding algorithm, and subsequently refined by solving a least-squares minimization problem (using the Levenberg–Marquardt algorithm). This iterative refinement was carried out using a custom-developed script that makes use of 7-parameter two-dimensional Gaussians and allows estimation of the atomic column peak positions with picometer precision [76, 77]. Then, polarization maps were calculated from the relative displace-

ments of the two cation sublattices present in the ferroelectric perovskite-type structures with general formula ABO_3 . Thus, the local ferroelectric polarization was calculated by measuring the polar displacement in the image plane of the B position from the center of mass of its four nearest A neighbors. Here, in the polarization maps derived from HAADF-STEM images, the polarization vectors are plotted opposite to the displacement of the B cations.

ACKNOWLEDGMENTS

N. A. S. acknowledges funding from the European Research Council (ERC) under the European Union's Horizon 2020 research and innovation programme grant agreement No 810451. I. E. and C. G. acknowledge the use of the Euler cluster managed by the HPC team at ETH Zurich. M. D. R. acknowledges support by the Swiss National Science Foundation under Project No 200021-175926, and is thankful to R. J. Zeches, P. Yu and R. Ramesh for the samples used in this study.

DATA AVAILABILITY

The data that support the findings of this study are available within the article.

-
- [1] M. Stengel, "Electrostatic stability of insulating surfaces: Theory and applications," *Phys. Rev. B* **84**, 205432 (2011).
- [2] D. D. Fong, A. M. Kolpak, J. A. Eastman, S. K. Streiffer, P. H. Fuoss, G. B. Stephenson, C. Thompson, D. M. Kim, K. J. Choi, C. B. Eom, I. Grinberg, and A. M. Rappe, "Stabilization of Monodomain Polarization in Ultrathin $PbTiO_3$ Films," *Phys. Rev. Lett.* **96**, 127601 (2006).
- [3] N. Sai, A. M. Kolpak, and A. M. Rappe, "Ferroelectricity in ultrathin perovskite films," *Phys. Rev. B* **72**, 020101(R) (2005).
- [4] R. V. Wang, D. D. Fong, F. Jiang, M. J. Highland, P. H. Fuoss, Carol Thompson, A. M. Kolpak, J. A. Eastman, S. K. Streiffer, A. M. Rappe, and G. B. Stephenson, "Reversible chemical switching of a ferroelectric film," *Phys. Rev. Lett.* **102**, 047601 (2009).
- [5] M. J. Highland, T. T. Fister, D. D. Fong, P. H. Fuoss, Carol Thompson, J. A. Eastman, S. K. Streiffer, and G. B. Stephenson, "Equilibrium polarization of ultrathin $PbTiO_3$ with surface compensation controlled by oxygen partial pressure," *Phys. Rev. Lett.* **107**, 187602 (2011).
- [6] P. Gao, Z. Zhang, M. Li, R. Ishikawa, B. Feng, H.-J. Liu, Y.-L. Huang, N. Shibata, X. Ma, S. Chen, J. Zhang, K. Liu, E.-G. Wang, D. Yu, L. Liao, Y.-H. Chu, and Y. Ikuhara, "Possible absence of critical thickness and size effect in ultrathin perovskite ferroelectric films," *Nat. Comm.* **8**, 1–8 (2017).
- [7] M. F. Chisholm, W. Luo, M. P. Oxley, S. T. Pantelides, and H. N. Lee, "Atomic-scale compensation phenomena at polar interfaces," *Phys. Rev. Lett.* **105**, 197602 (2010).
- [8] S. V. Levchenko and A. M. Rappe, "Influence of ferroelectric polarization on the equilibrium stoichiometry of lithium niobate (0001) surfaces," *Phys. Rev. Lett.* **100**, 256101 (2008).
- [9] M. Setvin, M. Reticioli, F. Poelzleitner, J. Hulva, M. Schmid, L. A. Boatner, C. Franchini, and U. Diebold, "Polarity compensation mechanisms on the perovskite surface $KTaO_3(001)$," *Science* **359**, 572–575 (2018).
- [10] N. Strkalj, G. De Luca, M. Campanini, S. Pal, J. Schaab, C. Gattinoni, N. A. Spaldin, M. D. Rossell, M. Fiebig, and M. Trassin, "Depolarizing-Field Effects in Epitaxial Capacitor Heterostructures," *Phys. Rev. Lett.* **123**, 147601 (2019).
- [11] C. Gattinoni, N. Strkalj, R. Hürdi, M. Fiebig, M. Trassin, and N. A. Spaldin, "Interface and surface stabilization of the polarization in ferroelectric thin films," *Proc. Nat. Acad. Sci.* (2020), 10.1073/pnas.2007736117.
- [12] K. Garrity, A. Kakekhani, A. Kolpak, and S. Ismail-Beigi, "Ferroelectric surface chemistry: First-principles study of the $PbTiO_3$ surface," *Phys. Rev. B* **88**, 045401 (2013).
- [13] J. Junquera and P. Ghosez, "Critical thickness for ferroelectricity in perovskite ultrathin films," *Nature* **422**, 506–509 (2003).
- [14] K. Ishikawa, T. Nomura, N. Okada, and K. Takada, "Size effect on the phase transition in $PbTiO_3$ fine particles," *Jap. J. Appl. Phys.* **35**, 5196–5198 (1996).
- [15] J. A. Mundy, G. B. F., C. A. Heikes, D. F. Segedin, Z. Wang, B. H. Goodge, Q. N. Meier, C. T. Nelson, B. Prasad, L. F. Kourkoutis, W. D. Ratcliff, N. A. Spaldin, R. Ramesh, and D. G. Schlom, arXiv.org (2020), 1812.09615.
- [16] R. D. King-Smith and D. Vanderbilt, "First-principles investigation of ferroelectricity in perovskite compounds," *Phys. Rev. B* **49**, 5828–5844 (1994).
- [17] N. A. Spaldin, "A beginner's guide to the modern theory of polarization," *J. Sol. Stat. Chem.* **195**, 2 (2012).
- [18] David Vanderbilt and R. D. King-Smith, "Electric polarization as a bulk quantity and its relation to surface charges," *Phys. Rev. B* **48**, 4442–4455 (1993).
- [19] A. Ohtomo and H. Y. Hwang, "A high-mobility electron gas at the $LaAlO_3/SrTiO_3$ heterointerface," *Nature* **427**, 423–426 (2004).
- [20] N. Nakagawa, H. Y. Hwang, and D. A. Muller, "Why some interfaces cannot be sharp," *Nature Mater.* **5**, 204–209 (2006).
- [21] N. Reyren, S. Thiel, A. D. Caviglia, L. Fitting Kourkoutis, G. Hammerl, C. Richter, C. W. Schneider, T. Kopp, A. S. Ruetschi, D. Jaccard, M. Gabay, D. A. Muller, J. M. Triscone, and J. Mannhart, "Supercon-

- ducting interfaces between insulating oxides,” *Science* **317**, 1196–1199 (2007).
- [22] M. F. Sarott, M. Fiebig, and M. Trassin, “Tracking ferroelectric domain formation during epitaxial growth of PbTiO_3 films,” *Appl. Phys. Lett.* **117**, 132901 (2020).
- [23] D. D. Fong, G. B. Stephenson, S. K. Streiffer, J. A. Eastman, O. Auciello, P. H. Fuoss, and C. Thompson, “Ferroelectricity in ultrathin perovskite films,” *Science* **304**, 1650–1653 (2004).
- [24] A. Lubk, M. D. Rossell, J. Seidel, Q. He, S. Y. Yang, Y. H. Chu, R. Ramesh, M. J. Hytch, and E. Snoeck, “Evidence of sharp and diffuse domain walls in BiFeO_3 by means of unit-cell-wise strain and polarization maps obtained with high resolution scanning transmission electron microscopy,” *Phys. Rev. Lett.* **109**, 047601 (2012).
- [25] S. Y. Yang, J. Seidel, S. J. Byrnes, P. Shafer, C. H. Yang, M. D. Rossell, P. Yu, Y. H. Chu, J. F. Scott, J. W. Ager, L. W. Martin, and R. Ramesh, “Above-bandgap voltages from ferroelectric photovoltaic devices,” *Nat. Nanotechnol.* **5**, 143–147 (2010).
- [26] M. G. Stachiotti and M. Sepiarsky, “Toroidal ferroelectricity in PbTiO_3 nanoparticles,” *Phys. Rev. Lett.* **106**, 137601 (2011).
- [27] A. K. Yadav, C. T. Nelson, S. L. Hsu, Z. Hong, J. D. Clarkson, C. M. Schlepüetz, A. R. Damodaran, P. Shafer, E. Arenholz, L. R. Dedon, D. Chen, A. Vishwanath, A. M. Minor, L. Q. Chen, J. F. Scott, L. W. Martin, and R. Ramesh, “Observation of polar vortices in oxide superlattices,” *Nature* **530**, 198 (2016).
- [28] A. R. Damodaran, J. D. Clarkson, Z. Hong, H. Liu, A. K. Yadav, C. T. Nelson, S. L. Hsu, M. R. McCarter, K. D. Park, V. Kravtsov, A. Farhan, Y. Dong, Z. Cai, H. Zhou, P. Aguado-Puente, P. Garcia-Fernandez, J. Iniguez, J. Junquera, A. Scholl, M. B. Raschke, L. Q. Chen, D. D. Fong, R. Ramesh, and L. W. Martin, “Phase coexistence and electric-field control of toroidal order in oxide superlattices,” *Nature Mat.* **16**, 1003 (2017).
- [29] S. Das, Y. L. Tang, Z. Hong, M. A. P. Gonçalves, M. R. McCarter, C. Klewe, K. X. Nguyen, F. Gómez-Ortiz, P. Shafer, E. Arenholz, V. A. Stoica, S. L. Hsu, B. Wang, C. Ophus, J. F. Liu, C. T. Nelson, S. Saremi, B. Prasad, A. B. Mei, D. G. Schlom, J. Iniguez, P. Garcia-Fernandez, D. A. Muller, L. Q. Chen, J. Junquera, L. W. Martin, and R. Ramesh, “Observation of room-temperature polar skyrmions,” *Nature* **568**, 368–372 (2019).
- [30] M. Stengel, C. J. Fennie, and P. Ghosez, “Electrical properties of improper ferroelectrics from first principles,” *Phys. Rev. B* **86**, 094112 (2012).
- [31] G. De Luca, N. Strkalj, S. Manz, C. Bouillet, M. Fiebig, and M. Trassin, “Nanoscale design of polarization in ultrathin ferroelectric heterostructures,” *Nat. Commun.* **8**, 1419 (2017).
- [32] M. Dawber, P. Chandra, P. B. Littlewood, and J. F. Scott, “Depolarization corrections to the coercive field in thin-film ferroelectrics,” *J. Phys. Cond. Matt.* **15**, L393–L398 (2003).
- [33] Y. S. Kim, D. H. Kim, J. D. Kim, Y. J. Chang, T. W. Noh, J. H. Kong, K. Char, Y. D. Park, S. D. Bu, J. G. Yoon, and J. S. Chung, “Critical thickness of ultrathin ferroelectric BaTiO_3 films,” *Appl. Phys. Lett.* **86**, 102907 (2005).
- [34] D. A. Tenne, P. Turner, J. D. Schmidt, M. Biegalski, Y. L. Li, L. Q. Chen, A. Soukiassian, S. Trolier-McKinstry, D. G. Schlom, X. X. Xi, D. D. Fong, P. H. Fuoss, J. A. Eastman, G. B. Stephenson, C. Thompson, and S. K. Streiffer, “Ferroelectricity in Ultrathin BaTiO_3 Films: Probing the Size Effect by Ultraviolet Raman Spectroscopy,” *Phys. Rev. Lett.* **103**, 177601 (2009).
- [35] D. Puggioni, G. Giovannetti, and J. M. Rondinelli, “Polar metals as electrodes to suppress the critical-thickness limit in ferroelectric nanocapacitors,” *J. Appl. Phys.* **124**, 174102 (2018).
- [36] A. Kakekhani and S. Ismail-Beigi, “Ferroelectric oxide surface chemistry: water splitting via pyroelectricity,” *J. Mater. Chem. A* **4**, 5235–5246 (2016).
- [37] Harold Y. Hwang, “Tuning interface states,” *Science* **313**, 1895–1896 (2006).
- [38] M. Stengel and D. Vanderbilt, “Berry-phase theory of polar discontinuities at oxide-oxide interfaces,” *Phys. Rev. B* **80**, 241103 (2009).
- [39] A. F. Santander-Syro, C. Bareille, F. Fortuna, O. Copie, M. Gabay, F. Bertran, A. Taleb-Ibrahimi, P. Le Fèvre, G. Herranz, N. Reyren, M. Bibes, A. Barthélémy, P. Lecoeur, J. Guevara, and M. J. Rozenberg, “Orbital symmetry reconstruction and strong mass renormalization in the two-dimensional electron gas at the surface of KTaO_3 ,” *Phys. Rev. B* **86**, 121107 (2012).
- [40] P. D. C. King, R. H. He, T. Eknapakul, P. Buaphet, S.-K. Mo, Y. Kaneko, S. Harashima, Y. Hikita, M. S. Bahramy, C. Bell, Z. Hussain, Y. Tokura, Z.-X. Shen, H. Y. Hwang, F. Baumberger, and W. Meevasana, “Subband structure of a two-dimensional electron gas formed at the polar surface of the strong spin-orbit perovskite KTaO_3 ,” *Phys. Rev. Lett.* **108**, 117602 (2012).
- [41] J. B. Neaton, C. Ederer, U. V. Waghmare, N. A. Spaldin, and K. M. Rabe, “First-principles study of spontaneous polarization in multiferroic BiFeO_3 ,” *Phys. Rev. B* **71**, 014113 (2005).
- [42] I. Efe, N. A. Spaldin, and C. Gattinoni, “On the happiness of ferroelectric surfaces and its role in water dissociation: The example of bismuth ferrite,” *J. Chem. Phys.* **154**, 024702 (2021).
- [43] P. Yu, W. Luo, D. Yi, J. X. Zhang, M. D. Rossell, C.-H. Yang, L. You, G. Singh-Bhalla, S. Y. Yang, Q. He, Q. M. Ramasse, R. Erni, L. W. Martin, Y. H. Chu, S. T. Pantelides, S. J. Pennycook, and R. Ramesh, “Interface control of bulk ferroelectric polarization,” *Proc. Nat. Acad. Sci.* **109**, 9710–9715 (2012).
- [44] M. Stengel and N. A. Spaldin, “Origin of the dielectric dead layer in nanoscale capacitors,” *Nature* **443**, 679–682 (2006).
- [45] P. Maksymovych, N. Balke, S. Jesse, M. Huijben, R. Ramesh, A. P. Baddorf, and S. V. Kalinin, “Defect-induced asymmetry of local hysteresis loops on BiFeO_3 surfaces,” *J. Mater. Sci.* **44**, 5095–5101 (2009).
- [46] Y. Shuai, S. Zhou, D. Bürger, M. Helm, and H. Schmidt, “Nonvolatile bipolar resistive switching in $\text{Au/BiFeO}_3/\text{Pt}$,” *J. Appl. Phys.* **109**, 124117 (2011).
- [47] M. Marinova, J. E. Rault, A. Gloter, S. Nemsak, G. K. Palsson, J.-P. Rueff, C. S. Fadley, C. Carrétéro, H. Yamada, K. March, V. Garcia, S. Fusil, A. Barthélémy, O. Stéphan, C. Colliex, and M. Bibes, “Depth profiling charge accumulation from a ferroelectric into a doped mott insulator,” *Nano Lett.* **15**, 2533–2541 (2015).
- [48] E. Bruyer, A. Sayede, A. Ferri, R. Desfeux, R. V. K. Mangalam, R. Ranjith, and W. Prellier, “Insight on the ferroelectric properties in a $(\text{BiFeO}_3)_2(\text{SrTiO}_3)_4$ superlattice from experiment and ab initio calculations,” *Appl.*

- Phys. Lett. **107**, 042904 (2015).
- [49] R. Ranjith, R. V. K. Mangalam, Ph. Boullay, A. David, M. B. Lepetit, U. Lüders, W. Prellier, A. Da Costa, A. Ferri, R. Desfeux, Gy. Vincze, Zs. Radi, and C. Aruta, “Constrained ferroelectric domain orientation in $(\text{BiFeO}_3)_m(\text{SrTiO}_3)_n$ superlattice,” Appl. Phys. Lett. **96**, 022902 (2010).
- [50] Y. Yang, C. M. Schlepütz, C. Adamo, D. G. Schlom, and R. Clarke, “Untilting BiFeO_3 : The influence of substrate boundary conditions in ultra-thin BiFeO_3 on SrTiO_3 ,” APL Mater. **1**, 052102 (2013).
- [51] W. Gao, C. Addiego, H. Wang, X. Yan, Y. Hou, D. Ji, C. Heikes, Y. Zhang, L. Li, H. Huyan, T. Blum, T. Aoki, Y. Nie, D. G. Schlom, R. Wu, and X. Pan, “Real-space charge-density imaging with sub-angstrom resolution by four-dimensional electron microscopy,” Nature **575**, 480–484 (2019).
- [52] Y. Yang, M. Stengel, W. Ren, X. H. Yan, and L. Bellaiche, “Epitaxial short-period $\text{PbTiO}_3/\text{BiFeO}_3$ superlattices studied by first-principles calculations,” Phys. Rev. B **86**, 144114 (2012).
- [53] Z. Zhang, P. Wu, L. Chen, and J. Wang, “First-principles prediction of a two dimensional electron gas at the $\text{BiFeO}_3/\text{SrTiO}_3$ interface,” Appl. Phys. Lett. **99**, 062902 (2011).
- [54] J. C. Yang, Q. He, S. J. Suresha, C. Y. Kuo, C. Y. Peng, R. C. Haislmaier, M. A. Motyka, G. Sheng, C. Adamo, H. J. Lin, Z. Hu, L. Chang, L. H. Tjeng, E. Arenholz, N. J. Podraza, M. Bernhagen, R. Uecker, D. G. Schlom, V. Gopalan, L. Q. Chen, C. T. Chen, R. Ramesh, and Y. H. Chu, “Orthorhombic BiFeO_3 ,” Phys. Rev. Lett. **109**, 247606 (2012).
- [55] Massimiliano Stengel and Jorge Íñiguez, “Electrical phase diagram of bulk BiFeO_3 ,” Phys. Rev. B **92**, 235148 (2015).
- [56] O. Dieguez, O. E. Gonzalez-Vazquez, Jacek C. Wojdel, and J. Iniguez, “First-principles predictions of low-energy phases of multiferroic BiFeO_3 ,” Phys. Rev. B **83**, 094105 (2011).
- [57] B. Carcan, H. Bouyanfif, M. El Marssi, F. Le Marrec, L. Dupont, C. Davoisne, J. Wolfman, and D. C. Arnold, “Phase Diagram of $\text{BiFeO}_3/\text{LaFeO}_3$ Superlattices: Antiferroelectric-Like State Stability Arising from Strain Effects and Symmetry Mismatch at Heterointerfaces,” Adv. Mater. Interfaces **4**, 1601036 (2017).
- [58] B. Carcan, H. Bouyanfif, M. El Marssi, F. Le Marrec, L. Dupont, C. Davoisne, J. Wolfman, and D. C. Arnold, “Interlayer strain effects on the structural behavior of $\text{BiFeO}_3/\text{LaFeO}_3$ superlattices,” J. Appl. Phys. **124**, 044105 (2018).
- [59] W. Sun, W. Wang, D. Chen, Z. Cheng, T. Jia, and Y. Wang, “Giant magnetoelectric coupling and two-dimensional electron gas regulated by polarization in $\text{BiFeO}_3/\text{LaFeO}_3$ heterostructures,” J. Phys. Chem. C , 16393–16399 (2019).
- [60] R. J. Zeches, M. D. Rossell, J. X. Zhang, A. J. Hatt, Q. He, C.-H. Yang, A. Kumar, C. H. Wang, A. Melville, C. Adamo, G. Sheng, Y.-H. Chu, J. F. Ihlefeld, R. Erni, C. Ederer, V. Gopalan, L. Q. Chen, D. G. Schlom, N. A. Spaldin, L. W. Martin, and R. Ramesh, “A Strain-Driven Morphotropic Phase Boundary in BiFeO_3 ,” Science **326**, 977–980 (2009).
- [61] A. J. Hatt, N. A. Spaldin, and C. Ederer, “Strain-induced isosymmetric phase transition in BiFeO_3 ,” Phys. Rev. B **81**, 054109 (2010).
- [62] M. D. Rossell, R. Erni, M. P. Prange, J.-C. Idrobo, W. Luo, R. J. Zeches, S. T. Pantelides, and R. Ramesh, “Atomic structure of highly strained BiFeO_3 thin films,” Phys. Rev. Lett. **108**, 047601 (2012).
- [63] L. Li, Y. Zhang, L. Xie, J. R. Jokisaari, C. Beekman, J.-C. Yang, Y.-H. Chu, H. M. Christen, and X. Pan, “Atomic-scale mechanisms of defect-induced retention failure in ferroelectrics,” Nano Lett. **17**, 3556–3562 (2017).
- [64] Y.-M. Kim, A.N. Morozovska, E.A. Eliseev, A.R. Lupini, Y.-H. Chu, P. Yu, R. Ramesh, S.J. Pennycook, S.V. Kalinin, A.Y. Borisevich, and et al., “Atomic structure of surface dielectric dead layer in BiFeO_3 thin film,” Microsc. Microanal. **19**, 1928–1929 (2013).
- [65] L. Jin, P. X. Xu, Y. Zeng, L. Lu, J. Barthel, T. Schulthess, R. E. Dunin-Borkowski, H. Wang, and C. L. Jia, “Surface reconstructions and related local properties of a BiFeO_3 thin film,” Sci. Reports **7**, 39698 (2017).
- [66] L. Xie, L. Li, C. A. Heikes, Y. Zhang, Z. Hong, P. Gao, C. T. Nelson, F. Xue, E. Kioupakis, L. Chen, D. G. Schlom, P. Wang, and X. Pan, “Giant ferroelectric polarization in ultrathin ferroelectrics via boundary-condition engineering,” Adv. Mater. **29**, 1701475 (2017).
- [67] H. Deniz, A. Bhatnagar, E. Pippel, R. Hillebrand, A. Hahnel, M. Alexe, and D. Hesse, “Nanoscale $\text{Bi}_2\text{FeO}_{6-x}$ precipitates in BiFeO_3 thin films: a metastable Aurivillius phase,” J. Mater. Sci. **49**, 6952–6960 (2014).
- [68] G. Kresse and J. Hafner, “*Ab initio* molecular dynamics for liquid metals,” Phys. Rev. B **47**, 558 (1993).
- [69] G. Kresse and J. Hafner, “*Ab initio* molecular-dynamics simulation of the liquid-metal–amorphous-semiconductor transition in germanium,” Phys. Rev. B **49**, 14251 (1994).
- [70] G. Kresse and J. Furthmüller, “Efficiency of *ab-initio* total energy calculations for metals and semiconductors using a plane-wave basis set,” Comp. Mat. Sci. **6**, 15 (1996).
- [71] G. Kresse and J. Furthmüller, “Efficient iterative schemes for *ab initio* total-energy calculations using a plane-wave basis set,” Phys. Rev. B **54**, 11169 (1996).
- [72] J. P. Perdew, A. Ruzsinszky, G. I. Csonka, O. A. Vydrov, G. E. Scuseria, L. A. Constantin, X. Zhou, and K. Burke, “Restoring the density-gradient expansion for exchange in solids and surfaces,” Phys. Rev. Lett. **100**, 136406 (2008).
- [73] M. Stengel, P. Aguado-Puente, N. A. Spaldin, and J. Junquera, “Band alignment at metal-ferroelectric interfaces: Insights and artifacts from first principles,” Phys. Rev. B **83**, 235112 (2011).
- [74] S. L. Dudarev, G. A. Botton, S. Y. Savrasov, C. J. Humphreys, and A. P. Sutton, “Electron-energy-loss spectra and the structural stability of nickel oxide: An LSDA+U study,” Phys. Rev. B **57**, 1505–1509 (1998).
- [75] G. Kresse and D. Joubert, “From ultrasoft pseudopotentials to the projector augmented-wave method,” Phys. Rev. B **59**, 1758 (1999).
- [76] A. B. Yankovich, B. Berkels, W. Dahmen, P. Binev, S. I. Sanchez, S. A. Bradley, A. Li, I. Szlufarska, and P. M. Voyles, “Picometre-precision analysis of scanning transmission electron microscopy images of platinum nanocatalysts,” Nat. Commun. **5**, 4155 (2014).

- [77] M. Campanini, R. Erni, C.-H. Yang, R. Ramesh, and M. D. Rossell, “Periodic giant polarization gradients in doped BiFeO_3 thin films,” *Nano Letters* **18**, 717–724 (2018).